Scale-by-scale turbulent energy budget in the intermediate wake of two-dimensional generators

F. Thiesset, R. A. Antonia, L. Danaila

Scale-by-scale turbulent energy budget in the intermediate wake of two-dimensional generators

F. Thiesset,[1, a)] R. A. Antonia,[1] and L. Danaila[2]

[1)] *School of Engineering, University of Newcastle, NSW 2308 Callaghan, Australia*

[2)] *CORIA, UMR 6614, Avenue de l'Université, BP 12, 76801 Saint Etienne du Rouvray, France*

It is first established, on the basis of new X-wire measurements, that the equilibrium similarity of the terms in the scale-by-scale (s-b-s) budget of the turbulent energy $\overline{q^2}$ is reasonably well approximated on the axis of the intermediate wake of a circular cylinder. The similarity, which scales on the Taylor microscale λ and $\overline{q^2}$, is then used to determine s-b-s energy budgets from the data of Antonia, Zhou & Romano[1] for 5 different two-dimensional wake generators. In each case, the budget is reasonably well closed, using the locally isotropic value of the mean energy dissipation rate, except near separations comparable to the wavelength of the coherent motion (CM). The influence of the initial conditions is first felt at a separation L_c identified with the cross-over between the energy transfer and large scale terms of the s-b-s budget. When normalized by $\overline{q^2}$ and L_c, the mean energy dissipation rate is found to be independent of the Taylor microscale Reynolds number. The CM enhances the maximum value of the energy transfer, the latter exceeding that predicted from models of decaying homogeneous isotropic turbulence.

PACS numbers: 47.27.nb, 47.27.De, 47.27.wb

[a)] Electronic mail: Email address : Fabien.Thiesset@newcastle.edu.au

I. INTRODUCTION

The concept of self-preservation, which effectively assumes that the flow is governed by single length and velocity scales, has an important role in describing the spatial evolution of turbulent flows. Implicit in this concept is the notion of forgetfulness or disentanglement from initial conditions. There is now however abundant evidence to suggest that initial conditions can influence the type of self-preservation that can be achieved in several types of turbulent flows, in particular free shear flows such as jets and wakes. The latter flows are especially interesting in view of the invariably strong organisation, in the form of vortical coherent structures, which is first observed immediately downstream of the wake-generating obstacle and which subsequently influences the streamwise development of the flow (*e.g.* Refs. 1–6).

Although the conditions for self-preservation, or sometimes self-similarity, have been investigated by considering the mean momentum and turbulent energy equations at one point in space, it is of course more powerful and general to consider the self-preservation of the two-point velocity correlation tensor. The precursor of this approach was outlined by Ref. 7 who obtained a similarity solution of the two-point velocity correlation for homogeneous isotropic turbulence when the Reynolds number is very large. George[8] proposed an equilibrium similarity solution of Lin's spectral equation, equivalent to the Kármán-Howarth equation, which is valid at any Reynolds number. This solution was tested in grid turbulence by Antonia *et al.*[9], in the context of the transport equation for the turbulent energy structure function $\overline{(\Delta q)^2} = \overline{(\Delta u)^2} + \overline{(\Delta v)^2} + \overline{(\Delta w)^2}$, where Δu, Δv, Δw are the velocity increments for u, v, w between two points separated by a distance r (*e.g.* $\Delta u = u(x+r) - u(x)$), and the overbar denotes time-averaging. A plausible interpretation of the transport equation of $\overline{(\Delta q)^2}$ is that it represents an energy budget at each scale, or a scale-by-scale (hereafter s-b-s) energy budget. There have been several attempts at investigating s-b-s budgets, using either experimental or numerical data, in other types of flows, *e.g.* in homogeneous shear flow[10–12], in the central region of a channel flow[13], in a circular jet[14–16], in wall-bounded flows[17,18]. In general, closure of the budget has been satisfactory validated by the data, allowing for the assumptions that are made when deriving the transport equations. In these previously cited flows, different physical phenomena are at play, for example grid turbulence is dominated by the advection of energy whilst diffusion is prominent near the centreline of a channel flow.

On the centreline of an axisymmetric jet, the major source of (large scale) inhomogeneity is associated with the streamwise decay of turbulent energy with only a small contribution from the production of energy arising from the difference in the Reynolds normal stresses.

In this paper, we examine the s-b-s energy budget in the intermediate wake of different obstacles. We focus on this region primarily because we expect the energy transfer in this region of the flow to be dominated, as in the case of grid turbulence and along the axis of a circular jet, by the streamwise decay of turbulent energy. However, unlike the latter two flows, one also expects that the transfer may feel the influence of the organised motion or coherent structures, the latter depending clearly on the type of initial condition, *viz.* the geometry of the wake-generating obstacle. Detailed velocity and vorticity measurements were made by Antonia, Zhou & Romano[1], hereafter AZR, at $x/d = 70$, in wakes generated by 5 different bluff-bodies, each with the same characteristic dimension d at nominally the same Reynolds number based on the Taylor microscale $R_\lambda \approx 200$. Unfortunately, there was no attempt in Ref. 1 at measuring the one point energy budget or establishing if similarity applied in this region of the flow. This would have enabled the construction of the the s-b-s energy budget. To remedy this shortcoming, we present new measurements made at several streamwise locations in the intermediate wake of a circular cylinder. Experimental details are given in section II. The one-point energy budget (section III) is then obtained and the equilibrium similarity is tested (section IV) and exploited in section V to examine the effect of initial conditions on the s-b-s energy budget. Finally, conclusions are drawn in section VI.

II. EXPERIMENTAL DETAILS

X-wire measurements were made in the wake of a circular cylinder in the CORIA wind tunnel, which is of recirculating type. The residual turbulence level is smaller than 0.2%. The square test section is $(0.4 \times 0.4\text{m}^2)$ has a length of 2.5m. The mean pressure gradient was set to zero. A circular cylinder of diameter $d = 10$mm, placed horizontally downstream the contraction, spanned the width of the test section. The upstream velocity U_0 was 6.5ms^{-1}, corresponding to a Reynolds number Re_d, based on the cylinder diameter, of 4333. Measurements of velocity fluctuations u and v were made at several streamwise locations in the range $40 \leq x/d \leq 110$. The X-wire probe (Dantec 55P51) was calibrated using a

look-up table technique (*e.g.* Refs. 19 and 20) with velocity and angle increment of 1ms^{-1} and 5^o respectively. The hot wires (Pt-W, 5μm diameter, 1.25mm length) were operated with a Dantec constant temperature bridge at an overheat ratio of 1.6. Voltage signals were passed though buck and amplifiers (SRS SIM983) and low-pass filtered (SRS SIM965) at a frequency f_c close to the Kolmogorov frequency $f_K \equiv \overline{U}/2\pi\eta$ ($\overline{U}$ is the local mean velocity and the Kolmogorov length-scale $\eta = (\nu^3/\overline{\epsilon})^{1/4}$). The sampling frequency $f_s = 20kHz$ and the sampling period was about 4min. The air temperature in the wind tunnel was kept constant during the calibration and measurements using a regulating cross-flow water-air cooler system which allowed the mean temperature to be controlled to $\pm 0.5^oC$.

Measurements made at the University of Newcastle in the wakes downstream of 5 different two dimensional obstacles, each with the same characteristic dimension $d = 25.4$mm have been detailed in Refs. 1 and 21. Only a brief description is given below (see Fig. 1).

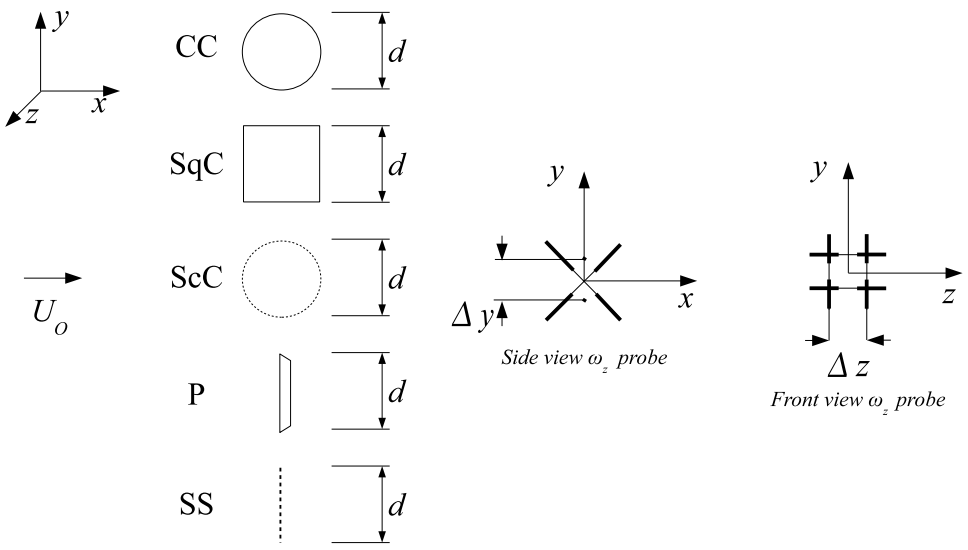

FIG. 1. Cross section of the five different generators used for the experiments carried out in Newcastle by Ref. 1. From top to bottom: CC, SqC, ScC, P, SS. Also sketched is a one-component vorticity probe in the ω_z configuration (ω_z is the vorticity component in the z direction).

The data were obtained in an open circuit wind tunnel with a 2.4m long square test section ($0.35 \times 0.35\text{m}^2$). The five generators (a circular cylinder CC, a square cylinder SqC, a screen cylinder ScC, a solid plate P normal to the flow and a screen strip SS, Fig. 1) were located 20cm downstream of the end of the contraction and spanned the width of the test

section. All measurements were made on the centreline at $x = 70d$ at several values of Re_d. A one-component vorticity probe (Fig. 1), which included an X-wire straddled by 2 parallel hot wires, was used to determine either ω_z when the X-wire was in the plane (x,y) or ω_y when the X-wire was in the (x,z) plane. All the hot wires were etched from Pt-10%Rh to a diameter of 2.5μm and an active length of approximatively 0.5mm (length to diameter ratio ≈ 200). They were operated at an overheat ratio of 1.5 with in-house constant temperature anemometers. The anemometer output signals were passed through buck and gain circuits, prior to low-pass filtering at a frequency $f_c \approx f_K$. The filtered signals were then digitized at a frequency $f_s = 2f_c$ into a PC using a 12bit A-D converter. The sampling period was in the range 45 to 100s. The mean velocity U_0, upstream of the wake generator, was varied so that the Taylor microscale Reynolds number R_{λ_u} ($\equiv \overline{u^2}^{1/2}\lambda_u/\nu$, where $\lambda_u = 15\nu\sqrt{\overline{u^2}/\overline{\epsilon}}$ is the Taylor microscale) was in the range $150 \lesssim R_{\lambda_u} \lesssim 300$ at $x/d = 70$.

III. ONE-POINT ENERGY BUDGET

It is important that the one-point energy budget is known relatively accurately since it represents the limiting state, as the separation r approaches the integral scale, of the s-b-s energy budgets. Here, we focus on the region along the axis of the intermediate wake. The general formulation of the one-point energy budget is

$$\frac{1}{2}\overline{U}_i\frac{\partial\overline{q^2}}{\partial x_i} + \overline{u_iu_j}\frac{\partial\overline{U_i}}{\partial x_j} + \frac{1}{2}\frac{\partial}{\partial x_j}\left(2\overline{u_jp} + \overline{u_jq^2}\right) + \overline{\epsilon} = 0. \qquad (1)$$

(the summation convention applies). The first term on left hand side of Eq. (1) represents the advection of turbulent kinetic energy by the mean velocity. The second term is interpreted as the production of kinetic energy through the mean velocity gradient. The third term corresponds to the diffusion of turbulent energy while the last term is the mean energy dissipation rate.

Profiles along the y axis of $\overline{vq^2}$ approximated by $2\overline{vu^2} + \overline{v^3}$ indicated that the diffusion of $\overline{q^2}$ by v is negligible along the axis since $\overline{vq^2} \approx$ constant on either side of the axis. A similar conclusion was arrived at by examining the data supplied to us by Zhou[22]. The latter measurements were made with a 3-component vorticity probe at $x/d = 10$, 20 and 40. These data, with simultaneous information for u, v and w, indicated that $\overline{vq^2}$ was more closely approximated by $2\overline{vu^2} + \overline{v^3}$ than by $\overline{vu^2} + 2\overline{v^3}$, *i.e.* axisymmetry with respect to y is

superior to that with respect to x. The latter axisymmetry along the y axis for large-scale statistics contrasts with Ref. 23 who observed a local axisymmetry with respect to the x axis at the level of the smallest scales. However, the present result appears reasonable since the influence of the Bénard-von Kármán street (a large-scale effect), which induces flow along the y direction cannot be neglected in this region of the wake.

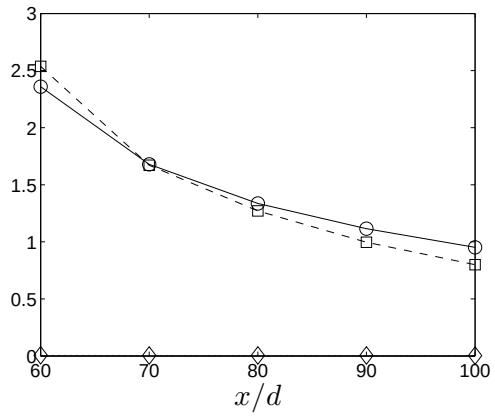

FIG. 2. Terms of the one-point kinetic energy budget (Eq. (2)) on the center-line of the wake of a circular cylinder normalized by U_0^3/d. □ $-\frac{1}{2}\overline{U}\frac{\partial \overline{q^2}}{\partial x}$, ○ $\overline{\epsilon}$, ♢ $\left(\overline{u^2}-\overline{v^2}\right)\frac{\partial \overline{U}}{\partial x}$.

With the assumption that diffusion by the pressure p is also negligible on the axis, the one-point energy budget Eq. (1) reduces to

$$\frac{1}{2}\overline{U}\frac{\partial \overline{q^2}}{\partial x}+\left(\overline{u^2}-\overline{v^2}\right)\frac{\partial \overline{U}}{\partial x}+\overline{\epsilon}=0 \tag{2}$$

The distributions (Fig. 2) indicate that the production term associated with the difference in the Reynolds normal stresses is negligible. Consequently, Eq. (2) further simplifies to

$$\frac{1}{2}\overline{U}\frac{\partial \overline{q^2}}{\partial x}+\overline{\epsilon}=0 \tag{3}$$

Although Fig. 2 shows that the advection and energy dissipation rate data crossover at $x/d=70$, the magnitude of the two distributions are sufficiently close to each other to claim that the energy budget over this range of x/d is quite similar to that for decaying homogeneous isotropic turbulence (or HIT), as approximated by a turbulent grid flow. This is a considerable simplification in the context of estimating the s-b-s energy budget since only the decay term needs to be taken into account when r is sufficiently large.

IV. SCALE-BY-SCALE ENERGY BUDGETS

In view of the analogy with decaying turbulence HIT, the s-b-s budget is in essence provided by the Kármán-Howarth equation[7] as detailed in Ref. 9. The latter authors assumed equilibrium similarity, as proposed by Ref. 8. The similarity scales are λ and $\overline{q^2}$. $\overline{q^2}$ decays according to a power-law, whose exponent depends on the initial conditions. Second- and third-order structure functions, as they appear in the following transport equation[24,25]

$$-\overline{\Delta u(\Delta q)^2} + 2\nu\frac{\partial}{\partial r}\overline{(\Delta q)^2} - \frac{\overline{U}}{r^2}\int_0^r s^2\frac{\partial}{\partial x}\overline{(\Delta q)^2}ds = \frac{4}{3}\epsilon r, \tag{4}$$

may be written as

$$f_q(\widetilde{r}) = \frac{\overline{(\Delta q)^2}}{\overline{q^2}}, \qquad g_q(\widetilde{r}) = -\overline{\Delta u(\Delta q)^2}\frac{3^{1/2}R_\lambda}{(\overline{q^2})^{3/2}} \tag{5}$$

where $\tilde{r} = r/\lambda$ and s in Eq. (4) is a dummy integration variable. Note that f_q and g_q depend only on $\tilde{r}$. Using Eq.(5), Eq. (4) can be rewritten as

$$g_q + 2f_q' - \left(\frac{5\Gamma_{q1}}{m_q} - 10\Gamma_{q2}\right)\widetilde{r}^{-2} = \frac{20}{3}\widetilde{r} \tag{6}$$

where

$$\Gamma_{q1} = \int_0^{\widetilde{r}} \widetilde{s}^3 f_q' d\widetilde{s}, \qquad \Gamma_{q2} = \int_0^{\widetilde{r}} \widetilde{s}^2 f_q d\widetilde{s}. \tag{7}$$

The prime denotes differentiation with respect to $\tilde{r}$. The parameter m_q is the power-law decay exponent of $\overline{q^2}$, *i.e.*

$$\overline{q^2} \propto (x - x_0)^{m_q} \tag{8}$$

where x_0 is a virtual origin. Eq. (3) implies that $\overline{\epsilon}$ will also decay in a power-law fashion

$$\overline{\epsilon} \propto (x - x_0)^{m_\epsilon} \tag{9}$$

with $m_\epsilon = m_q - 1$. Since $\lambda^2 = 5\nu\overline{q^2}/\overline{\epsilon}$, it follows that the exponent m_λ, *viz.*

$$\lambda \propto (x - x_0)^{m_\lambda} \tag{10}$$

should be equal to 0.5. The expected linearity of λ^2 with respect to x was used to estimate x_0 ($\approx 8d$). The distributions, along the wake centreline of $\overline{u^2}$, $\overline{q^2}$, $\overline{\epsilon}$, λ and $\overline{U}_d^2$ ($\overline{U}_d$ is the maximum velocity defect) are shown in Fig. 3. Note that m_{U_d} ($\overline{U}_d^2 \propto (x - x_0)^{m_{U_d}}$) is -0.68, which is substantially different from the value of -1, expected in the far wake. Also R_λ

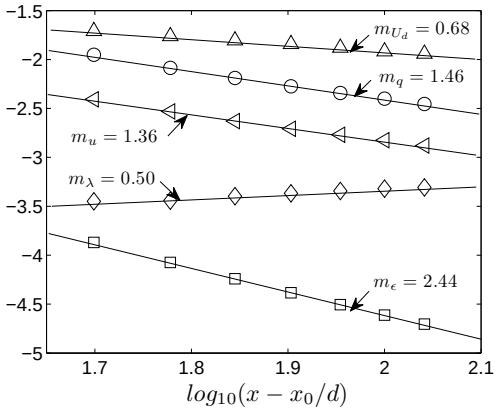

FIG. 3. Decay exponents on the wake center-line of the circular cylinder wake ; ○ $log_{10}(\overline{q^2}/U_0^2)$, ◁ $log_{10}(\overline{u^2}/U_0^2)$, □ $log_{10}(\overline{\epsilon}d/U_0^3)$, ♢ $log_{10}(10^{-1}\lambda/d)$, △ $log_{10}(U_d^2/U_0^2)$, solid lines are linear fits to the data.

must decay with x through the intermediate wake ($R_\lambda \propto (x - x_0)^{-0.23}$) whereas it should be independent of x in the far wake.

For convenience, Eqs.(6) can be rewritten as

$$G_q + D_q + I_q = \frac{4}{3} \tag{11}$$

where $G_q = g_q \tilde{r}^{-1}/5$, $D_q = 2f_q' \tilde{r}^{-1}/5$ and $I_q = -\left(\Gamma_{q1}/m_q - 2\Gamma_{q2}\right)\widetilde{r}^{-3}$. Each term can be estimated from measurements made at one spatial location provided m_q is available.

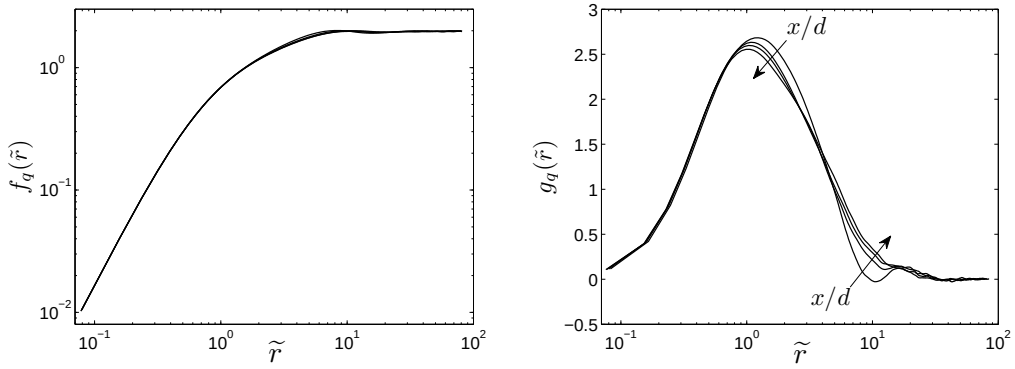

(a) (b)

FIG. 4. (a) f_q and (b) $g_q/\tilde{r}$ as a function of $\tilde{r}$, for x between $50d$ and $110d$ of the circular cylinder wake.

Measured distributions of f_q in Fig. 4(a) confirm that the collapse, based on λ and $\overline{q^2}$, is quite satisfactory. Note that f_q approaches its limiting value (= 2) at large $\tilde{r}$ after overshooting it, due mainly to the contribution from $\overline{(\Delta v)^2}$, which is affected by the coherent motion[21]. The quality of the collapse for g_q (Fig. 4(b)) is not as good as that in Fig. 4(a); it is however at least as good, if not better, than that reported by Ref. 9 for grid turbulence. Note also that the curve of g_q at $x = 50d$ differs quite significantly from those beyond $x = 70d$ for which the collapse is much more satisfactory irrespectively of the downstream distance. Particularly, at a separation $\tilde{r} \approx 10$, g_q reaches negative values which is most likely due to the presence of the organized motion. This may highlight that a transition in the behaviour of the coherent motion occurs between $x = 50d$ and $70d$.

V. RESULTS FOR SCALE-BY-SCALE ENERGY BUDGETS IN THE 5 WAKES

Since all measurements in the five different wakes were made[1] at only one streamwise location ($x/d = 70$), equilibrium similarity, which was verified in the previous section for the wake of the circular cylinder, will be used, together with the value of m_q reported in Fig. 3, to construct the s-b-s budgets for these 5 wakes. Although one would expect some dependence of m_q on both Re_d and the initial conditions, we have assumed that it remains constant for the present purpose, since its influence on the s-b-s energy budget, especially for $R_\lambda \approx 200$ is likely to be small.

We first consider the distributions of f_q (Fig. 5) for the five different wakes. The main point which emerges from this figure is that the effect of initial conditions cannot be discounted, at least when $\tilde{r}$ is sufficiently large. The collapse at small $\tilde{r}$ is almost as good as that reported at small $r^*(\equiv r/\eta)$ in Fig. 7 of[1], where $\overline{(\Delta u^*)^2}$ and $\overline{(\Delta v^*)^2}$ were plotted as functions of r^* (the asterisk stands for the normalization by the Kolmogorov scales). However, although Kolmogorov scaling may be superior in the dissipative range, scaling on λ and $\overline{q^2}$ extends the collapse to a wider range of scales. In general, distributions for different wakes depart from each other at $\tilde{r} \approx 2$. Note also the significant overshoot in $f_q = \overline{(\Delta q)^2}/\overline{q^2}$ for the screen strip (SS) with a maximum at $\tilde{r} = 12$. Included in Fig. 5 are the distributions (thin and bold curves) obtained from the models of Kurien & Sreenivasan[26] (hereafter KS) and Aivalis *et al.*[27] (henceforth A). The latter models rely on a parametric equation for

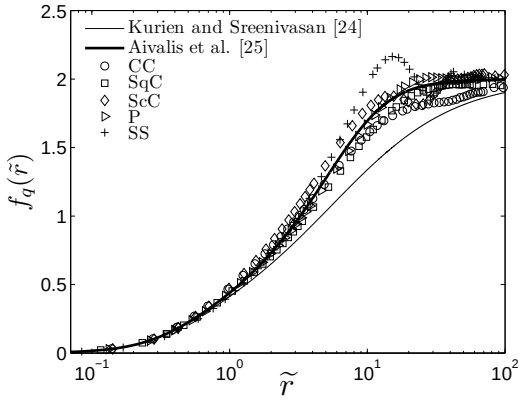

FIG. 5. Measured distributions of f_q as a function of $\tilde{r}$ for the five different wakes. Also shown is f_q inferred from KS[26] (thin line) and A[27] (bold line). The Taylor microscale Reynolds number is approximatively the same in each case, *viz.* $R_{\lambda_u} \approx 195$. ○ CC, □ SqC, ♢ ScC, ▷ P, + SS.

second-order structure functions

$$\overline{(\Delta u)^{*2}}|_K = \frac{r^{*2}}{15}\frac{(1+\beta r^*)^{(2c-2)}}{(1+\alpha r^{*2})^c} \tag{12}$$

$$\overline{(\Delta u)^{*2}}|_A = \frac{r^{*2}}{15}\frac{(1+(\beta r^*)^2)^{(c-1)}}{(1+\alpha r^{*2})^c}, \tag{13}$$

where the subscript K and A refer to the models of KS[26] and A[27] respectively. In Eqs. (12) and (13), $\beta = L^{*-1}$ where $L^* = C_\epsilon R_\lambda^{3/2} 15^{-3/4}$ ($C_\epsilon = 1$ as in Refs. 9 and 28) is a measure of the integral length-scale. $\alpha = (15C_u)^{-3/2}$ ($C_u = 2$ was chosen[9,28]) designates the cross-over between the dissipative and inertial range. Finally, $c = 1 - \zeta_u/2$ where ζ_u is the inertial range exponent of the longitudinal second order structure function. In contrast to Danaila *et al.*[29] or Thiesset *et al.*[30], for which ζ_u is function of the turbulent Reynolds number R_λ, we assume here $\zeta_u = 2/3$ as in Refs. 9 and 28. Then, $\overline{(\Delta q)^2}$ is calculated using the isotropic relation

$$\overline{(\Delta q)^{*2}}|_{K,A} = (3 + r^*\frac{\partial}{\partial r^*})\overline{(\Delta u)^{*2}}|_{K,A}. \tag{14}$$

After inserting Eq. (14) in Eq. (11), one can calculate the third-order structure function by difference. These models are thus only parametrized by the Reynolds number R_λ and the decay exponent m_q.

A comparison of Eqs.(13) and (12) indicates that the two models differ only through their

numerator, *i.e.*

$$\frac{\overline{(\Delta u)^{*2}}|_K}{\overline{(\Delta u)^{*2}}|_A} = \left[\frac{1+2\beta r^*+(\beta r^*)^2}{1+(\beta r^*)^2}\right]^{(c-1)} \tag{15}$$

As $c<1$, $\overline{(\Delta q)^{*2}}|_K < \overline{(\Delta q)^{*2}}|_A$ for every separation r as observed in Fig. 5. Thus, $I_q|_K < I_q|_A$ and so $G_q|_K > G_q|_A$. Nevertheless, in the limit of large scales

$$\lim_{r\to\infty}\overline{(\Delta q)^{*2}}|_K = \lim_{r\to\infty}\overline{(\Delta q)^{*2}}|_A = \frac{6R_\lambda}{15^{1/2}} \tag{16}$$

and for small separations

$$\lim_{r\to 0}\overline{(\Delta q)^{*2}}|_K = \lim_{r\to 0}\overline{(\Delta q)^{*2}}|_A = \frac{r^{*2}}{3} \tag{17}$$

Therefore, the two models lead to a same asymptotic distributions of energy in the limit of small and large separations. The main difference between the two models occurs at intermediate scales.

We now turn our attention to the different terms in the s-b-s energy budgets displayed in Fig. 6. All the terms in Eq. (11) are shown in this figure. Differences in the budgets between the 5 wakes tend to occur when $\tilde{r} \geq 2$. This separation corresponds approximatively to the cross-over L_c (identified by vertical arrow in Fig. 6) between the transfer term and the large scale decay or inhomogeneous term. It follows that the energy distribution becomes more sensitive to the initial conditions the larger $\tilde{r}$ is by comparison to L_c. This distribution is more influenced by the contribution of the relatively organized large scales which are more likely to remember the initial conditions.

G_q is much more affected by whether the wake generator is porous or solid than the other terms. For the porous wakes, the magnitude of G_q remains larger than that predicted by the two models when $\tilde{r} \geq 2$. This reflects the relatively strong organization in these two wakes and hence the stronger influence of the initial conditions. Note that the A[27] model fails to adequately represent G_q in these two cases (for $\tilde{r} \geq 2$) whereas it represents adequately the other terms (I_q and D_q) and is superior to the KS model[26]. The sum $G_q + I_q + D_q$ is close to the expected value of 4/3 for the solid generators. There is however a significant departure, typically in the range $2 \leq \tilde{r} \leq 10$, for the porous generators and especially SS. For these two wakes, the local anisotropy is greater than for the other 3 wakes[21], reflecting the larger degree of organisation in the porous generator wakes than in the impervious generator wakes[21].

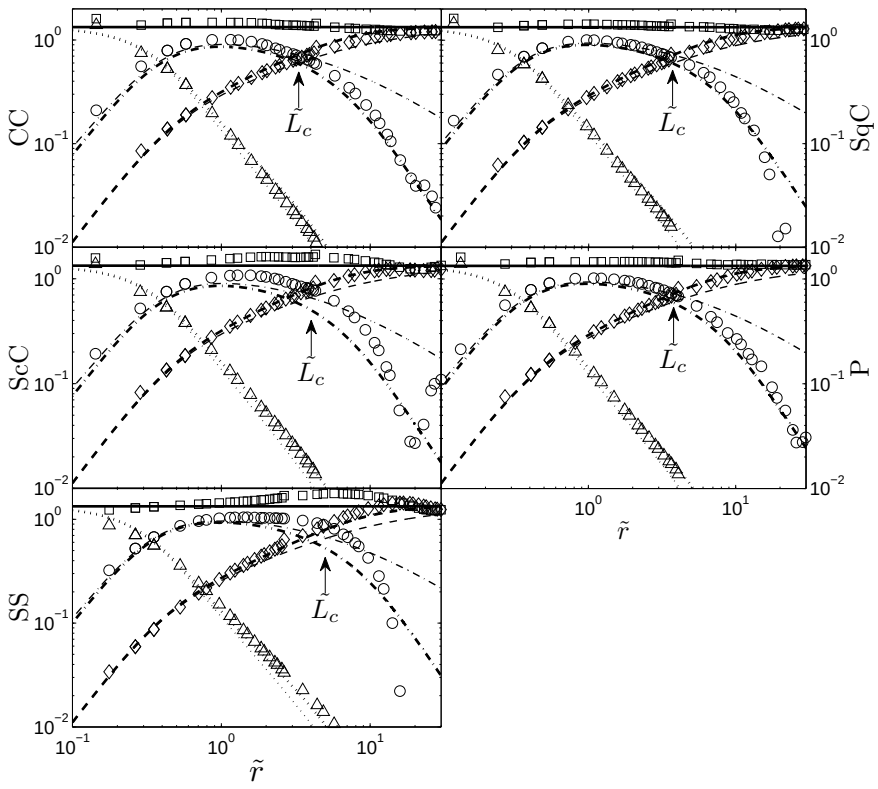

FIG. 6. Scale-by-scale energy budgets Eq. (11) in the five different wakes. Thin curves correspond to the model of KS[26] and bold curves to the model of A[27]. Symbols denote the experimental data. ○ , — · —: G_q; ▷, ·····: D_q; ♢, - - - -: I_q; □, ——: $(G_q + D_q + I_q)$. The thick horizontal line corresponds to 4/3.

The crossover length scale L_c has been identified with the separation at which $G_q = I_q$. From Eq. (6), we can thus write

$$\tilde{L_c} = \left[\frac{1}{g_q(\tilde{L_c})} \left(\frac{5\Gamma_{q1}(\tilde{L_c})}{m_q} - 10\Gamma_{q2}(\tilde{L_c}) \right) \right]^{1/2} . \tag{18}$$

One expects $\tilde{L_c}$ to depend on initial conditions since g_q, Γ_{q1}, Γ_{q2} and m_q should all be affected by the initial conditions. A plausible interpretation of L_c is that it represents a length scale at which the energy injected in the system starts being transferred towards small scales. It thus seems appropriate to normalize the mean energy dissipation rate $\overline{\epsilon}$ by L_c and $\overline{q^2}$, *i.e.*

$$\overline{\epsilon} = C_{\epsilon c} \frac{\left(\overline{q^2}/3\right)^{3/2}}{L_c}. \tag{19}$$

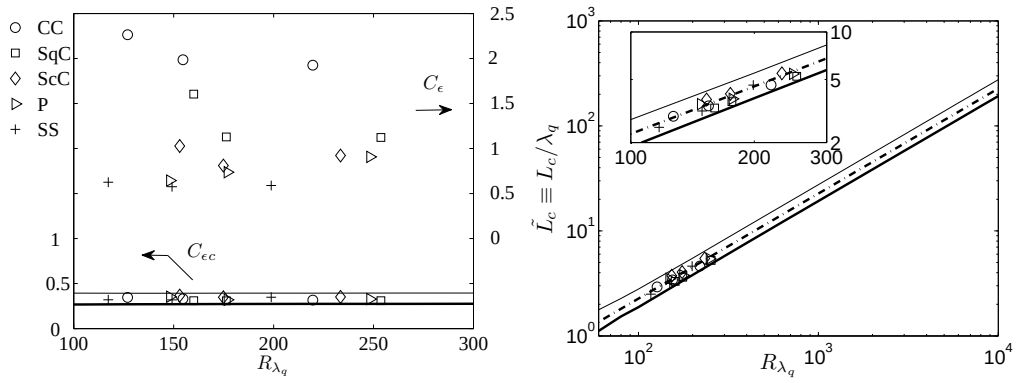

(a) (b)

FIG. 7. (a) Evolution of the normalized dissipation rate parameters C_ϵ and $C_{\epsilon c}$ with R_λ for the five wakes. Also presented is the expectation for $C_{\epsilon c}$ using either the model of A[27] (thick lines) or KS[26] (thin lines). (b) Evolution of the crossover length scale L_c normalized by λ with the Taylor microscale Reynolds number R_λ. Models; —— A[27] (thick lines), —— KS[26] (thin lines), — · — $L_s/\lambda_q = C_{\epsilon_c} R_{\lambda q}/15$ using $C_{\epsilon c} = 0.34$. Experiments ○ CC, □ SqC, ♢ ScC, ▷ P, + SS.

This differs from the classical definition of the normalized dissipation rate parameter C_ϵ

$$\overline{\epsilon} = C_\epsilon \frac{\left(\overline{u^2}\right)^{3/2}}{L_u}, \tag{20}$$

where L_u is the longitudinal integral length-scale. Fig. 7(a) shows the evolution of the normalized dissipation rate parameter, defined with either Eq. (20) or (19). As was emphasized by Ref. 1, C_ϵ reaches very different values depending on the type of obstacle. Indeed, C_ϵ is equal to about 2 for CC wake and has a quite different value (≈ 0.6) in the SS wake. On the other hand, when the normalization of $\overline{\epsilon}$ is based on L_c and $\overline{q^2}$, $C_{\epsilon c}$ appears to be remarkably universal, *i.e.* it is independent of both the type of obstacle and the Reynolds number. The constancy of $C_{\epsilon c}$ is also reasonably well reproduced by the two models. The measured value of $C_{\epsilon c}$ is equal to 0.34 whereas the values predicted by the KS and A models are equal to 0.28 and 0.4 respectively.

It is evident that $C_{\epsilon c}$ has a much stronger claim to universality than C_ϵ. This is due in part to the fact that L_c is much more precisely determined than L_u but more importantly because L_c is an intermediate scale between that at which energy is injected into the flow and that ($r \sim \lambda$) at which the transfer of energy is maximum. In other words, the cross-over between G_q and I_q defines the scale at which the energy associated with all the inhomogeneous large

scales, arising from the way energy is injected into the flow, is exactly balanced by the energy transferred to the dissipative scales.

The use of L_c and $\overline{q^2}$ as the normalization scales for the normalized dissipation rate parameter has two main practical advantages. First, replacing $\overline{u^2}$ by $\overline{q^2}$ allows the large-scale anisotropy to be accounted for. Second, the estimation of L_c is much less arbitrary than that of L_u, the latter being usually inferred by integrating the longitudinal correlation function to its first zero crossing.

It seems more appropriate to consider the ratio L_c/λ since λ is the scale at which the energy transfer is maximum. This ratio can be thought of as a measure of the separation between large scale and inertial range effects. By using Eq. (19) and since $\lambda_q = 5\nu\overline{q^2}/\overline{\epsilon}$, we obtain

$$L_c/\lambda_q = \frac{1}{15} C_{\epsilon c} R_{\lambda_q}. \tag{21}$$

The magnitude of $\tilde{L}_c$, identified with the values of $\tilde{r}$ for which $G_q = I_q$ is shown in Fig. 7(b). Also included in this figure are the values of $\tilde{L}_c$ which correspond to the two models. $\tilde{L}_c$ is always smaller for the A model[27] than for the KS model[26]. The measured values of $\tilde{L}_c$ lie between the two models; although the range of R_λ is small, all the data are quite consistent with a linear variation of $\tilde{L}_c$ with R_λ and are very close to the line $L_c/\lambda_q = C_{\epsilon_c} R_{\lambda_q}/15$.

The interpretation for L_c provided here is similar to that for the shear length-scale L_S, first introduced by Corrsin[31] in the context of shear-dominated flows, and further physically interpreted in Refs. 11, 17, 18, and 32. Indeed, the authors emphasized that $L_S \equiv \sqrt{S^3/\overline{\epsilon}}$[31] corresponds to the crossover between contributions from the production term due to the mean shear S and the nonlinear transfer term in the spherically averaged scale-by-scale kinetic energy budget. Note also that the present authors have recently generalized the definition of L_S in order to account for the additional effect of the coherent strain using similar arguments as in Ref. 11, *i.e.* based on scale-by-scale budgets (see Ref. 21). This suggests that there exists a large variety of different relevant injection length-scales depending on the flow under consideration. For example, as far as wake flows are concerned, L_c and L_S coexist, L_c being the crossover between the decay term and the transfer term and L_S the crossover between the production (due to both the mean shear and the coherent shear) and the transfer term.

In addition, even though we observe that L_c restores universality for the dissipation rate,

its applicability for modeling the dissipation rate has the shortcoming that this applies only to decaying flows. In shear-dominated turbulence, L_S is likely to be the relevant injection length-scale for normalizing the dissipation rate. This point is worth investigating in the future.

Finally, L_c represents the largest length-scale that is in essence affected by the shape of the obstacle. Therefore, as shown in Ref. 32 for shear flows, for a proper implementation of a Large Eddy Simulation (LES), L_c represents the threshold scale that has to be simulated, scales smaller than L_c having the best prospect of being modeled by a universal function.

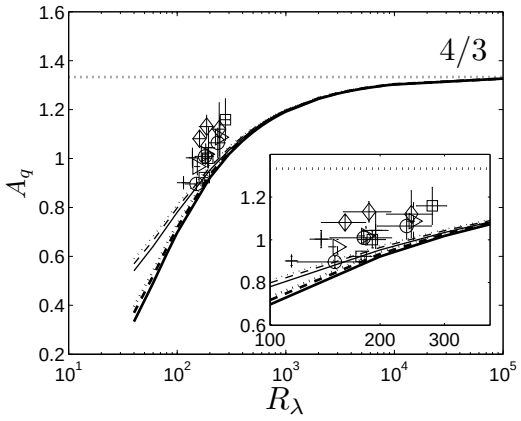

FIG. 8. Evolution of A_q with R_λ and the effect of m_q on A_q. Thick and thin curves correspond to the models of A[27] and KS[26] respectively. ——: $m_q = 1.25$, - - - -: $m_q = 1.5$, ·····: $m_q = 1.75$. ○ CC, □ SqC, ♢ ScC, ▷ P, + SS.

We now turn our attention to the maximum value of the energy transfer $A_q \equiv \max(\overline{\Delta u(\Delta q)^2}/\overline{\epsilon} r)$ depicted in Fig. 8. Vertical and horizontal error bars are also given in order to appraise uncertainties in assessing A_q. Vertical error bars correspond to the standard deviation between different (isotropic) estimations of the dissipation rate. From the one-component vorticity probe oriented in either the $x-y$ plane or $x-z$ plane, one can calculate $\overline{\epsilon}$ from

the following six expressions

$$\overline{\epsilon}_{iso} = 15\nu\overline{\left(\frac{\partial u}{\partial x}\right)^2} \tag{22}$$

$$\overline{\epsilon}_q = 3\nu\left[\overline{\left(\frac{\partial u}{\partial x}\right)^2} + \overline{\left(\frac{\partial v}{\partial x}\right)^2} + \overline{\left(\frac{\partial w}{\partial x}\right)^2}\right] \tag{23}$$

$$\overline{\epsilon}_{\omega_z} = \nu\left(2\overline{\omega_z^2} + \overline{\omega_y^2}\right) \tag{24}$$

$$\overline{\epsilon}_{\omega_y} = \nu\left(\overline{\omega_z^2} + 2\overline{\omega_y^2}\right) \tag{25}$$

$$\overline{\epsilon}_{xy} = \nu\left[6\overline{\left(\frac{\partial u}{\partial x}\right)^2} + 3\overline{\left(\frac{\partial u}{\partial y}\right)^2} + 2\overline{\left(\frac{\partial v}{\partial x}\right)^2} + \overline{\left(\frac{\partial u}{\partial y}\frac{\partial v}{\partial x}\right)}\right] \tag{26}$$

$$\overline{\epsilon}_{xz} = \nu\left[6\overline{\left(\frac{\partial u}{\partial x}\right)^2} + 3\overline{\left(\frac{\partial u}{\partial z}\right)^2} + 2\overline{\left(\frac{\partial w}{\partial x}\right)^2} + \overline{\left(\frac{\partial u}{\partial z}\frac{\partial w}{\partial x}\right)}\right]. \tag{27}$$

Vertical error bars can thus be interpreted as a measure of anisotropy at the level of the smallest scales. A_q is calculated using $\overline{\epsilon}_{iso}$ which appears to be close to the mean value between these 6 different surrogates. Horizontal error bars are calculated from the difference between $R_{\lambda_u} = \sqrt{\overline{u^2}}\lambda_u/\nu$ and $R_{\lambda_q} = \sqrt{\overline{q^2}}\lambda_q/\sqrt{3}\nu$, where $\lambda_u^2 = 15\nu\overline{u^2}/\overline{\epsilon}_{iso}$ and $\lambda_q^2 = 5\nu\overline{q^2}/\overline{\epsilon}_{iso}$. The ratio between R_{λ_u} and R_{λ_q} is thus

$$\frac{R_{\lambda_u}}{R_{\lambda_q}} = \sqrt{\frac{3\overline{u^2}}{\overline{q^2}}}\left(\frac{\lambda_u}{\lambda_q}\right) = \frac{3\overline{u^2}}{\overline{q^2}} \tag{28}$$

which gives a measure of the anisotropy at the largest scales. Measured values of A_q are also compared together with those inferred from the A and KS models, for three different values of m_q (1.25, 1.5 and 1.75). Note that variations in the magnitude of m_q has virtually no effect on the way A_q approaches the asymptote of 4/3. The influence of the decay exponent is more discernible when R_λ is small, as the contribution from the large scale term becomes more pronounced. For R_λ larger than 100, the differences are not perceptible and the choice of a single value of m_q for the 5 wakes seems therefore reasonable.

Measured values of A_q are systematically larger than those predicted from the models of decaying isotropic turbulence by on average 15%. The two porous obstacles, for which CM is more prominent, appear to produce a higher maximum value of the energy transfer, independently of the Reynolds number. This observation indicates that the energy transfer is affected by the presence of the coherent motion, whose effect is to locally enhance the cascade mechanism. A similar observation was made by Ref. 33, for the wake of a circular cylinder at $x = 40d$ and a smaller Reynolds number ($R_\lambda \approx 70$).

VI. CONCLUSIONS

There are three major conclusions which arise from this work, all pertaining to the intermediate region of a turbulent wake.

(i) Firstly, the X-wire measurements at various streamwise locations along the axis of the wake indicate that equilibrium similarity, based on the Taylor microscale λ and the turbulent energy $\overline{q^2}$, is verified satisfactorily. In particular, the collapse of the energy transfer term $\overline{\Delta\tilde{u}(\Delta\tilde{q})^2}R_\lambda\overline{q^2}^{-3/2}\tilde{r}^{-1}$ appears to be of better quality than that previously obtained for decaying turbulence downstream a grid[9]. In the intermediate wake and for large separations, the one-point energy budget is closely approximated by a balance between advection and energy dissipation rate. This is substantially different to what is generally observed in the far field[34] in which the diffusion term has also to be taken into account. This difference between the intermediate and far wake might be related to a reorganization or rescaling of the large-scale structures[4,35,36], sometimes referred to as the secondary vortex street. Further investigations of velocity statistics and corresponding length-scales obtained over a sufficiently large distance between the near and far fields are needed to confirm this.

(ii) Secondly, the equilibrium similarity is used to estimate the s-b-s budgets, also along the centreline, for wakes generated by five two-dimensional bodies of different shapes. The closure of the budgets is less satisfactory for the two porous bodies (screen strip and screen cylinder) than for the solid bodies (cylinder, plate and square), reflecting the persistence of the coherent motion arising from the Kelvin-Helmholtz instability in the shear layers associated with the porous bodies.

Initial conditions are first felt at a separation L_c, which corresponds to the intersection point between the energy transfer and the large scale terms. For $r < L_c$, the shape of the generator is not important and the statistics are similar to those for decaying homogeneous isotropic turbulence. The parameter $C_{\epsilon c}$ which involves normalization by L_c and $\overline{q^2}$, is remarkably independent of R_λ and almost unaffected by the initial conditions. Clearly, the ramification of this universality and its possible extension to other flows deserves to be investigated further. L_c/λ varies linearly with R_λ, a result in accord with existing models of $\overline{(\Delta q)^2}$ as well as our measurements.

(iii) Finally, the maximum value of the energy transfer term is systematically larger than that predicted by models for decaying HIT. This reflects the presence of the coherent

motion. The latter observation is important in the context of providing some insight into the way the coherent motion interacts with small scales. Some progress has been made on this interaction[33], by quantifying the contribution of the coherent motion to the energy transfer after writing the s-b-s budgets for both the coherent and random motions.

ACKNOWLEDGMENTS

The financial support of the 'Agence Nationale de la Recherche' (ANR), under the projects 'ANISO' and 'MUVAR', is gratefully acknowledged. RAA is grateful to the Australian Research Council for its support. We thank T. Zhou for carrying out the original Newcastle experiments.

REFERENCES

[1]R. A. Antonia, T. Zhou, and G. P. Romano, "Small-scale turbulence characteristics of two-dimensional bluff body wakes," J. Fluid Mech. **459**, 67–92 (2002).

[2]P. Bevilaqua and P. S. Lykoudis, "Turbulence memory in self-preserving wakes," J. Fluid Mech. **89**, 589–606 (1978).

[3]I. Wygnanski, F. Champagne, and B. Marasli, "On the large-scale structures in two-dimensional, small-deficit, turbulent wakes," J. Fluid Mech. **168**, 31–71 (1986).

[4]J. M. Cimbala, H. M. Nagib, and A. Roshko, "Large structure in the far wakes of two-dimensional bluff bodies," J. Fluid Mech. **190**, 265–298 (1988).

[5]Y. Zhou and R. A. Antonia, "Memory effects in a turbulent plane wake," Exp. Fluids **19**, 112–120 (1995).

[6]R. A. Antonia and J. Mi, "Approach towards self-preservation of turbulent cylinder and screen wakes," Exp. Therm. Fuid. Sci. **17**, 277–284 (1998).

[7]T. von Kármán and L. Howarth, "On the statistical theory of isotropic turbulence," Proc. Roy. Soc. Lond. A **164 (917)**, 192–215 (1938).

[8]W. George, "The decay of homogeneous isotropic turbulence," Phys. Fluids **4**, 1492–1509 (1992).

[9]R. A. Antonia, R. J. Smalley, T. Zhou, F. Anselmet, and L. Danaila, "Simi-

larity of energy structure functions in decaying homogeneous isotropic turbulence," J. Fluid Mech. **487**, 245–269 (2003).

[10]W. K. George and M. M. Gibson, "The self-preservation of homogeneous shear flow turbulence," Exp. Fluids **13**, 229–238 (1992).

[11]C. M. Casciola, P. Gualtieri, R. Benzi, and R. Piva, "Scale-by-scale budget and similarity laws for shear turbulence," J. Fluid Mech. **476**, 105–114 (2003).

[12]L. Danaila, F. Anselmet, and T. Zhou, "Turbulent energy scale-budget equations for nearly homogeneous sheared turbulence," Flow, Turbulence and Combustion **72**, 287–310 (2004).

[13]L. Danaila, F. Anselmet, and R. A. Antonia, "Turbulent energy scale budget equations in a fully developed channel flow," J. Fluid Mech. **430**, 87–109 (2001).

[14]D. Ewing and W. George, "Similarity analysis of the two-point velocity correlation tensor in a turbulent axisymmetric jet," Turbulence, Heat, and Mass Transfer **1**, 49–56 (1995).

[15]P. Burattini, R. A. Antonia, and L. Danaila, "Similarity in the far field of a turbulent round jet," Phys. Fluids **17**, 025101 (2005).

[16]P. Burattini, R. A. Antonia, and L. Danaila, "Scale-by-scale energy budget on the axis of a turbulent round jet." J. Turbulence **6**, 1–11 (2005).

[17]N. Marati, C. M. Casciola, and R. Piva, "Energy cascade and spatial fluxes in wall turbulence," J. Fluid Mech. **521**, 191–215 (2004).

[18]N. Saikrishnan, E. De Angelis, E. K. Longmire, I. Marusic, C. M. Casciola, and R. Piva, "Reynolds number effects on scale energy balance in wall turbulence," Phys. of Fluids **24**, 015101 (2012).

[19]L. Browne, R. A. Antonia, and L. P. Chua, "Calibration of X-probes for turbulent flow measurements," Exp. Fluids **7**, 201–208 (1989).

[20]P. Burattini and R. A. Antonia, "The effect of different x-wire schemes on some turbulence statistics," Exp. Fluids **38**, 80–89 (2005).

[21]F. Thiesset, L. Danaila, and R. A. Antonia, "Dynamical effect of the total strain induced by the coherent motion on local isotropy in a wake." J. Fluid Mech. **720**, 393–423 (2013).

[22]T. Zhou, Y. Zhou, M. Yiu, and L. Chua, "Three-dimensional vorticity in a turbulent cylinder wake," Exp. Fluids **35**, 459–471 (2003).

[23]J. Mi and R. A. Antonia, "Approach to local axisymmetry in a turbulent cylinder wake," Exp. Fluids **48**, 933–947 (2010).

[24]L. Danaila, F. Anselmet, and R. A. Antonia, "An overview of the effect of large scale inhomogeneities on small-scale turbulence," Phys. Fluids **14**, 2475–2484 (2002).

[25]L. Danaila, R. A. Antonia, and P. Burattini, "Progress in studying small-scale turbulence using 'exact' two-point equations," New J. Phys. **6**, 128 (2004).

[26]S. Kurien and K. R. Sreenivasan, "Anisotropic scaling contributions to high-order structure functions in high-Reynolds-number turbulence." Phys. Rev. E **62**, 2206–2212 (2000).

[27]K. G. Aivalis, K. R. Sreenivasan, Y. Tsuji, J. Klewicki, and C. A. Biltoft, "Temperature structure functions for air flow over moderately heated ground," Phys. Fluids **14**, 2439–2446 (2002).

[28]R. A. Antonia and P. Burattini, "Approach to the 4/5 law in homogeneous isotropic turbulence," J. Fluid Mech. **550**, 175–184 (2006).

[29]L. Danaila, R. A. Antonia, and P. Burattini, "Comparison between kinetic energy and passive scalar energy transfer in locally homogeneous isotropic turbulence," Phys. D **241**, 224–231 (2012).

[30]F. Thiesset, R. Antonia, and L. Danaila, "Restricted scaling range models for turbulent velocity and scalar energy transfers in decaying turbulence," Journal of Turbulence **14:3**, 25–41 (2013).

[31]S. Corrsin, "Local isotropy in turbulent shear flow," Tech. Rep. (NACA RM, 1958).

[32]P. Gualtieri, C. M. Casciola, R. Benzi, and R. Piva, "Preservation of statistical properties in large-eddy simulation of shear turbulence," J. Fluid Mech. **592**, 471–494 (2007).

[33]F. Thiesset, L. Danaila, R. A. Antonia, and T. Zhou, "Scale-by-scale budgets which account for the organised motion," J. Phys. Conference series **318**, 052040 (2011).

[34]L. W. B. Browne, R. A. Antonia, and D. A. Shah, "Turbulent energy dissipation in a wake," J. Fluid Mech. **179**, 307–326 (1987).

[35]R. A. Antonia, L. W. B. Browne, D. Bisset, and L. Fulachier, "A description of the organized motion in the turbulent far wake of a cylinder at low reynolds number," J. Fluid Mech. **184**, 423–44 (1987).

[36]G. Brown and A. Roshko, "Turbulent shear layers and wakes," J. Turbulence **13**, 1–32 (2012).